Rare Metal Materials and Engineering
Volume 54, Issue 8, August 2025
Available online at www.rmme.ac.cn

Science Press

Cite this article as: Qu Xingchen, Wang Xiaorong, Liu Xiaoqin, et al. Microstructure and Wear Properties of $AlCu_2(NiCr)_2Ti-(WC)_x$ HEA Composite Coatings on TC11 via Coincident CWW-Powder Plasma Cladding[J]. Rare Metal Materials and Engineering, 2025, 54(08): 1980-1987. DOI: https://doi.org/10.12442/j.issn.1002-185X.20240411.

ARTICLE

Microstructure and Wear Properties of $AlCu_2(NiCr)_2Ti-(WC)_x$ HEA Composite Coatings on TC11 via Coincident CWW-Powder Plasma Cladding

Qu Xingchen[1], Wang Xiaorong[1], Liu Xiaoqin[1], Liu Xiaoxiao[1], Meng Qian[2], He Peng[3]

[1] School of Mechanical and Electrical Engineering, Lanzhou Jiaotong University, Lanzhou 730010; [2] School of Materials Science and Engineering, Lanzhou Jiaotong University, Lanzhou 730010; [3] State Key Laboratory of Advanced Welding and Jointing, Harbin Institute of Technology, Harbin 150001

Abstract: The high-entropy alloy composite coatings $AlCu_2Ti(NiCr)_2-(WC)_x$ (x denotes powder feeding speeds, including 0, 25, 50, and 75 r/min) were prepared by plasma cladding using a hybrid mode of $AlCu_2(NiCr)_2Ti$ cable-type welding wire (CWW) and tungsten carbide (WC) powder. The effect of WC powder feeding speed on the microstructure, hardness, and wear properties of the prepared coatings was investigated. The results show that the coatings consist of body-centered cubic main phases and face-centered cubic secondary phases, with carbide reinforcement phases formed due to the addition of WC. The hardness and wear resistance of the coatings are significantly improved compared to the TC11 substrate. When WC powder feeding speed is set at 50 r/min, the coating exhibits optimal wear resistance, with a minimum volume wear rate of 8.5869×10^{-6} $mm^3\cdot N^{-1}\cdot m^{-1}$, greatly improving the wear properties of TC11 surface. The coincident CWW-powder plasma cladding provides a viable method for the preparation of high-entropy alloy composite coatings with enhanced wear resistance.

Key words: microstructure; metals and alloys; high-entropy alloy coating; plasma cladding; coincident CWW-powder

1 Introduction

The TC11 (Ti-6.5Al-3Mo-1.5Zr-0.25Si) titanium alloy exhibits remarkable characteristics, such as low density, high strength, and exceptional corrosion resistance[1]. Consequently, it finds extensive applications in aerospace, marine vessels, and biomedicine. However, insufficient wear resistance remains a significant issue for TC11[2–4]. Enhancing wear resistance by preparing wear-resistant coatings on the TC11 surface has become an effective solution[5–8]. In recent decades, high-entropy alloys (HEAs) have garnered considerable attention owing to their special bcc/fcc/hcp microstructure and excellent wear properties[9–12]. The preparation of HEA coatings by various surface engineering techniques is currently a hot research topic[11–15].

Plasma powder cladding has attracted significant interest for HEA coating preparation due to easy composition ratio adjustment and powder preparation[16]. According to previous studies, cladding coatings prepared using this method exhibit excellent metallurgical bonding with the substrate and high interfacial adhesion strength up to 800–950 MPa[17–19]. However, the low utilization rate of powder in plasma powder cladding is a major drawback[20]. Wire-feeding plasma cladding greatly improves material utilization, yet preparing HEA coatings using this method has been a challenge[21–23]. The emergence of cable-type welding wire (CWW) can facilitate HEA coating preparation via wire-feeding plasma cladding[24–25]. For instance, in-situ synthesized carbide-reinforced HEA coatings has been achieved via gas tungsten arc welding cladding using FeCuNiMoTiC CWWs, effectively improving the coating hardness and the wear resistance[26].

Received date: July 08, 2024
Foundation item: National Natural Science Foundation of China (51764038); Gansu Science and Technology Planning Project (2022JR5RA314, 22YF7WA151, 22YF7GA138, 23CXGA0151); Gansu Provincial Department of Education: Industrial Support Plan Project (2022CYZC-31); Gansu Provincial Association of Science and Technology Innovation Driving Force Project (GXH20230817-10)
Corresponding author: Wang Xiaorong, Ph. D., Professor, School of Mechanical and Electrical Engineering, Lanzhou Jiaotong University, Lanzhou 730010, P. R. China, Tel: 0086-931-4938023, E-mail: wxrlanzhou@126.com

$AlCu_2(NiCr)_2Ti$ CCWs are more economical and easier to prepare than other cladding materials, but they still exhibit issues such as large friction coefficients and high wear rates.

To address these problems, tungsten carbide (WC) modification of $AlCu_2(NiCr)_2Ti$ CWW was proposed. Metal matrix composites with WC are considered excellent strengthening materials due to their high hardness, strength, and wear resistance[25]. Previous research, such as the preparation of WC particle-reinforced high-entropy Fe-Co-Cr-Ni alloy composite coating using plasma cladding proposed by Peng et al[26], demonstrated significant improvements in wear resistance. Similarly, Gu et al[27] prepared WC-reinforced Fe-based composites through laser melting, and studied the effects of laser parameters on the density, microstructure, and mechanical properties of the materials.

However, there are few investigations on the preparation of HEA coatings by adding WC as a reinforcing phase in $AlCu_2(NiCr)_2Ti$ CWW using plasma cladding technique. In this work, a coincident CWW-powder plasma cladding method was proposed, combining paraxial CWW and coaxial carbide powder, to produce $AlCu_2Ti(NiCr)_2$-$(WC)_x$ (x denotes powder feeding speeds, including 0, 25, 50, and 75 r/min) HEA composite coatings. The related wear resistance mechanism was discussed from the microstructure evolution of the coating. This study is expected to provide a feasible solution for the problem of low hardness and poor wear resistance of TC11 titanium alloy, and to offer valuable insights for future applications of plasma cladding using the hybrid mode of CWW and powder.

2 Experiment

2.1 Preparation of cladding materials

Pure Cu wires (C>99at% , Φ0.5 mm), pure Al wires (Al>99at% , Φ0.5 mm), ERTi-2 pure Ti wires (Ti>99at% , Φ0.5 mm) and Ni80Cr20 alloy wires (consisting approximately of 22at% Cr and 78at% Ni, Φ0.5 mm) were used. The $AlCu_2(NiCr)_2Ti$ CWWs consist of six metal wires: one Al wire, two Cu wires, one Ti wire, and two NiCr, as depicted in Fig. 1b. CWWs were produced using a custom-designed stranding wire machine, as shown in Fig. 1b. WC powder (purity>99wt%, particle size: 100–150 μm), was dried in an electric heating oven at 100 ℃ for 2 h. TC11 plates with dimension of 100 mm×80 mm×5 mm were used as substrates, and their surfaces were cleaned by 800# sandpapers and alcohol wipes to remove the surface impurity and oil before cladding.

2.2 Preparation of $AlCu_2(NiCr)_2Ti$-$(WC)_x$ coatings

The plasma cladding experiments were conducted using a robotic plasma cladding system (Fig. 1a), which includes a serial industrial robot (YR-UP6-A00, MOTOMAN) and a plasma power source (DML-V02BD, Shanghai Duomu). The coincident CWW-powder plasma cladding is illustrated in Fig. 1b. The CWW was fed through a wire feeder while the WC powder was coaxially fed by a powder feeding system.

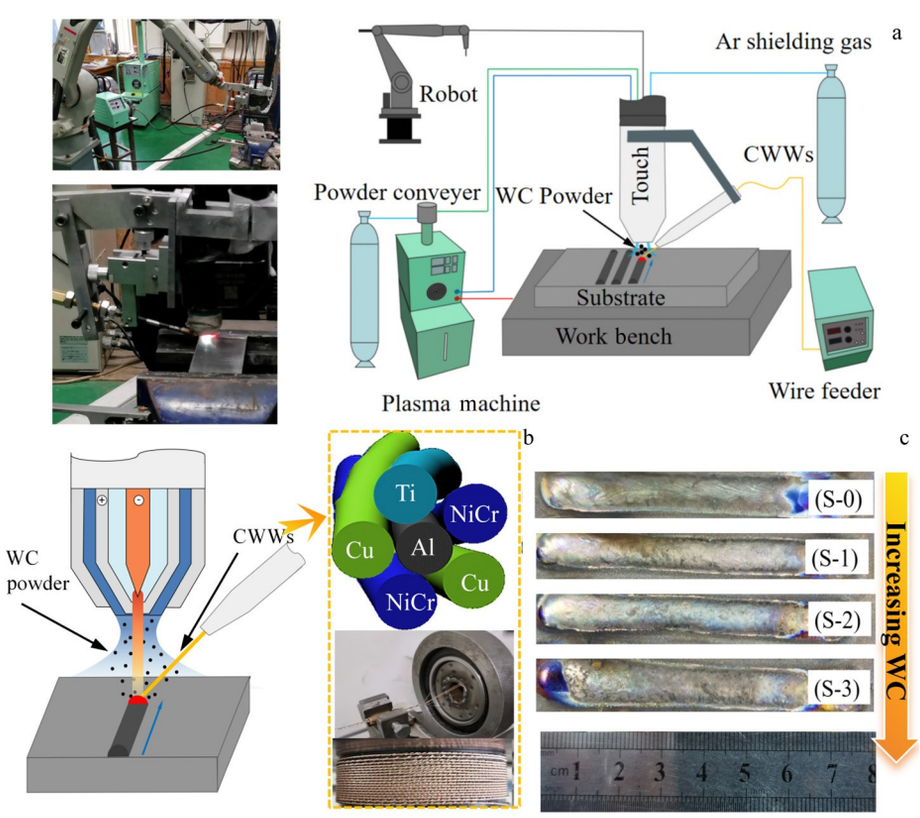

Fig.1 Robotic plasma cladding system (a); schematic of coincident CWW-powder plasma cladding and $AlCu_2(NiCr)_2Ti$-CWWs consisting of six metal wires (b); produced composite coatings (c)

The optimized process parameters are shown in Table 1. The $AlCu_2Ti(NiCr)_2$-$(WC)_x$ coatings prepared at powder feeding speeds (x) of 0, 25, 50, and 75 r/min were denoted as S-0, S-1, S-2, and S-3, respectively (Fig.1c).

2.3 Structure and property characterization

The microstructure and chemical composition of the prepared sample were analyzed using a field emission scanning electron microscope (SEM, Quanta 200FEG) equipped with an energy dispersive spectrometer (EDS). X-ray diffractometer (XRD, D8 ADVANCE) analysis was performed using a Cu kα radiation (λ=0.154 nm) and was operated at 40 kV and 40 mA. Diffraction patterns were obtained from 20° to 100° with a step size of 0.02° and a dwell time of 0.15 s. Hardness measurements were carried out by a Vickers hardness tester (HXD-1000TMB, Shanghai Fengming; load of 200g; time for 15 s). The samples were cut into cubes with 20 mm×15 mm×5 mm in dimension using an electric spark wire cutting machine for the wear performance testing, which was conducted by a friction and wear test machine (HT-1000, Lanzhou Kaihua). The basic structure of the test machine is illustrated in Fig. 2. A detection position was taken every 120°, and the average value of each sample was measured three times. The wear rate (W, $mm^3 \cdot N^{-1} \cdot m^{-1}$) of the sample was calculated according to Eq.(1):

$$W = \frac{V}{PL} \quad (1)$$

where V is the wear volume (mm^3), which can be obtained by $V=2\pi rA$ (A is the wear cross-sectional area and r is the friction radius); L is the total friction distance (m); P is the applied load (N). The particle size is within 100–150 μm.

Table 1 Plasma cladding parameters

Parameter	Value
Current/A	120
CWW feeding speed/mm·s^{-1}	8
Argon flow rate/L·min^{-1}	5
Cladding speed/mm·s^{-1}	3
Distance between the nozzle and the substrate surface/mm	5

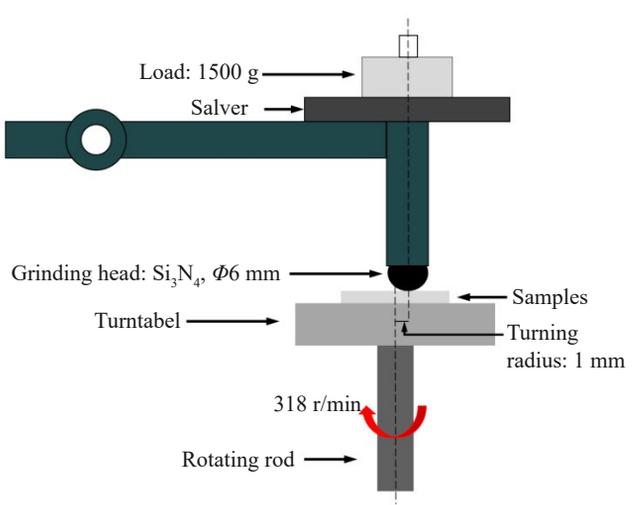

Fig.2 Schematic diagram of friction and wear test

3 Results and Discussion

3.1 Phase and microstructure

The XRD patterns of the $AlCu_2Ti(NiCr)_2$-$(WC)_x$ composite coatings are shown in Fig. 3a. The produced coatings are composed of bcc main phases and fcc secondary phases, exhibiting a preferred orientation to the (110) crystal plane. The diffraction peak of the (110) crystal plane is significantly higher than that of other peaks. This is attributed to the significant lattice distortion of the coatings and the thermal stress generated by the rapid cooling during the plasma cladding process, leading to substantial strain energy in the coatings. The (110) crystal plane, having the lowest surface energy, can adjust the excessive strain energy of the coating[26,28–29].

The enlarged XRD patterns of the samples at diffraction range from 38° to 44° are shown in Fig. 3b. With increasing the feeding speed of WC powder, the diffraction peak at around 40°, corresponding to (110) crystal plane, is gradually shifted to higher angles. Based on Bragg's law, the lattice parameters of S-0, S-1, S-2 and S-3 samples are 0.3976, 0.3965, 0.3960, and 0.3953 nm, respectively. The decrease in lattice spacings of the bcc phase is mainly attributed to the lattice distortion caused by the small atom size of the element C doped in the alloy[30–31]. As the overall C content in the coating increases, more C atoms are incorporated into the bcc structures, resulting in a decrease in lattice parameter[31–32].

Cross-sectional SEM images of $AlCu_2Ti(NiCr)_2$-$(WC)_x$ HEA composite coatings are shown in Fig. 4, indicating that the coatings contain α phase (dendrite phase), β phase (intergranular phase), and γ phase (granular phase), and the amount of γ phase increases with higher WC addition content. The relative intensity of the fcc phase is lower than that of the bcc phases, indicating a smaller volume fraction of the fcc phase. Thus, fcc phase corresponds to the β phase, while bcc phase corresponds to the α phase. According to EDS analysis results shown in Table 2, the α phase is Ti/Al-rich and Cu-depleted phase, while the β phase is Cu-rich. Additionally, the γ phase is inferred to be a WC/TiC based solid solution. The SEM images in Fig. 5 indicate that the coating is well bonded

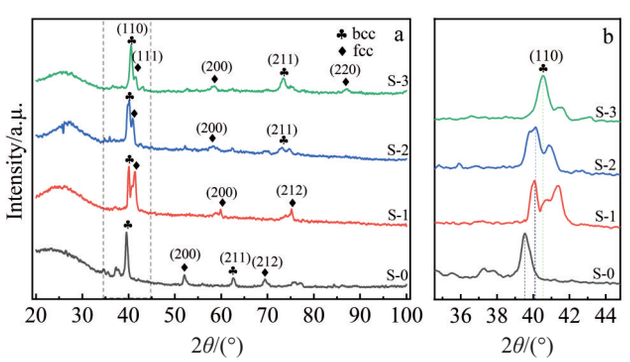

Fig.3 XRD patterns of $AlCu_2Ti(NiCr)_2$-$(WC)_x$ coatings (a); enlarged XRD patterns of bcc (110) peaks (b)

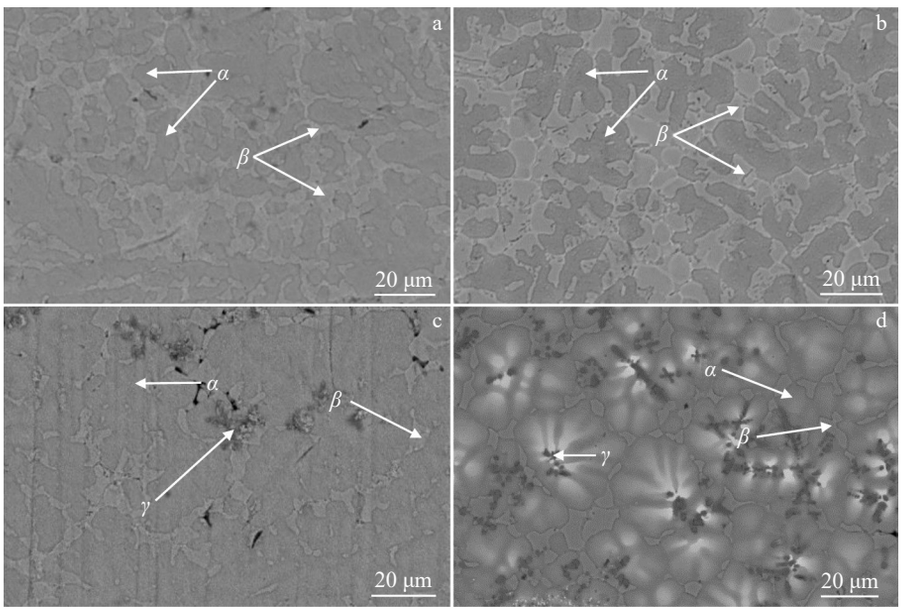

Fig.4 Cross-sectional SEM images of S-0 (a), S-1 (b), S-2 (c), and S-3 (d) samples

Table 2 Chemical composition of $AlCu_2Ti(NiCr)_2$-$(WC)_x$ HEA composite coatings

Sample	Powder feeding speed, x/r·min^{-1}	Region	Element/at%						
			Al	Cu	Cr	Ni	C	Ti	W
S-0	0	average	6.89	22.25	7.84	7.22	-	55.80	-
		α	13.40	12.00	6.90	6.10	-	61.60	-
		β	8.10	29.10	5.60	5.20	-	52.00	-
S-1	25	average	6.42	15.90	7.38	6.16	5.13	40.19	0.52
		α	12.60	10.00	6.00	8.00	7.60	55.40	0.40
		β	8.00	30.00	8.70	7.30	6.60	39.10	0.30
S-2	50	average	6.00	15.72	7.58	6.80	15.32	43.38	5.21
		α	12.10	9.70	6.00	6.90	9.60	52.70	3.00
		β	7.50	28.70	5.50	6.20	8.30	38.20	5.60
		γ	1.10	0.900	0.20	0.60	19.50	65.40	12.30
S-3	75	average	6.13	14.15	6.82	5.17	17.73	42.50	7.40
		α	11.80	8.50	5.70	4.90	9.30	53.90	5.90
		β	7.50	26.90	6.10	5.60	9.60	36.50	7.80
		γ	1.20	4.60	0.70	0.80	26.80	50.60	15.30

to the TC11 substrate, with a distinct fusion line. As WC content increases, the presence of γ phase is significantly enhanced, with a certain number of WC spherical particles appearing near the fusion line (Fig. 5c–5d). This results from the rapid cooling of the molten pool, preventing the complete melting of the WC powder with high melting point.

3.2 Hardness and wear properties

The Vickers hardness of the produced coatings is shown in Fig. 6. The average hardness values of the coatings are 751.4, 867.1, 892.0, and 944.0 $HV_{0.2}$ for S-0, S-1, S-2, and S-3 samples, respectively, which are positively correlated to the addition content of WC. In comparison, the hardness of HEA coatings is 2.0 – 2.6 times higher than that of the TC11 substrate, exhibiting immediate enhancement in mechanical properties. The hardness variation along the cross-section of the coating is due to the changes in microstructure of the HEA coatings[33]. The increase in WC content causes lattice distortion and raises the concentration of free elements W and C in HEA matrix after dissolution and diffusion of WC particles. The dissolution enhances solid solution strengthening effect, and more carbide phases are precipitated, which are generally hard and brittle. Thus, the hardness of the coating improves under the combined effects. Additionally, a sudden increase in hardness occurs at about 2 mm from the coating surface due to unmelted WC particles near the fusion line. WC, a common high-hardness strengthening phase, further contributes to the hardness of the coatings[34–35].

The coefficients of friction (COF) of the coatings (Fig. 7),

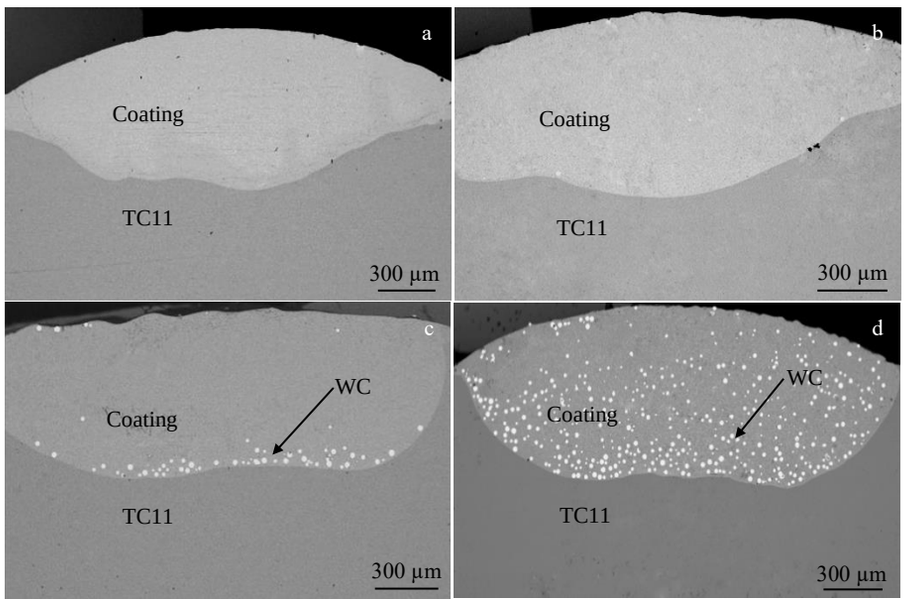

Fig.5 Overall cross-sectional morphologies of S-0 (a), S-1 (b), S-2 (c), and S-3 (d) samples

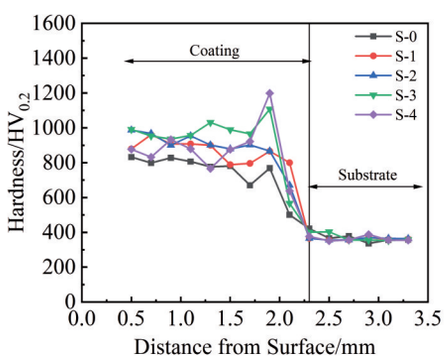

Fig.6 Vicker hardness of $AlCu_2Ti(NiCr)_2$-$(WC)_x$ HEA composite coatings

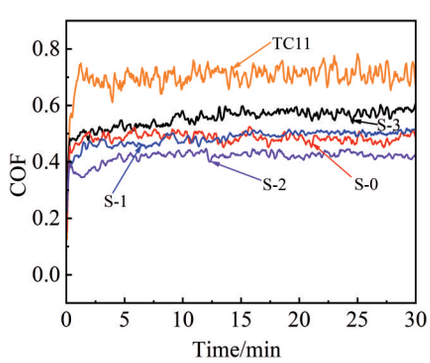

Fig.7 COF curves of $AlCu_2Ti(NiCr)_2$-$(WC)_x$ HEA composite coatings

are lower than that of the TC11. The TC11 substrate exhibits the highest average COF (about 0.71), while the coated TC11 samples show significantly improved COF: 0.48 (S-0), 0.47 (S-1), 0.39 (S-2), and 0.52 (S-3). The lowest COF of sample S-2 (x=50 r/min) is attributed to the hard WC particles, which have high hardness, good wear resistance, and strong deformation resistance during friction[36–37], and are not easy to deform plastically, thus stabilizing the COF curves[38]. However, when the powder feeding speed reaches 75 r/min, the COF increases slightly due to the reduced volume fraction of the HEA matrix. The bonding degree between HEA matrix and WC particles decreases, leading to the peeling of WC particles during the friction process.

The wear rates of the samples are shown in Fig.8. The wear resistance of the coatings initially increases and then decreases with higher WC content. The TC11 substrate has a volume wear rate of 12.6439×10^{-6} $mm^3\cdot N^{-1}\cdot m^{-1}$. The coatings improve the wear resistance to varying degrees, with the minimum wear rate (8.5869×10^{-6} $mm^3\cdot N^{-1}\cdot m^{-1}$) observed at x=50 r/min, which is 32% lower than that of the TC11 titanium alloy. However, at x=75 r/min, the wear rate slightly increases, potentially due to the cracks on the surface of the coating, causing WC particles to break and to peel off[39].

3.3 Probable wear resistance mechanism

To investigate the wear resistance mechanism of $AlCu_2$-$(NiCr)_2Ti$-$(WC)_x$ HEA composite coatings on TC11, the worn

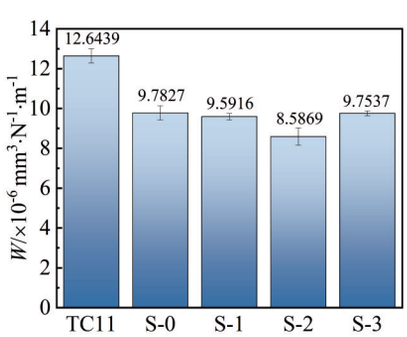

Fig.8 Wear rate (W) histograms of $AlCu_2Ti(NiCr)_2$-$(WC)_x$ HEA composite coatings

morphologies of the TC11 substrates and the coatings are shown in Fig. 9. The TC11 substrate shows severe wear with significant spalling and small abrasive particles of various shapes and sizes, indicating abrasive wear. Abrasive wear features include distinct furrows or wear debris on the friction surface (Fig. 9a), resulting from the cutting effect, plastic deformation, fatigue damage, or brittle fracture of the abrasive particles on the friction surface.

For S-0 sample (x=0 r/min), the wear marks are shallow, but some debris is present (Fig.9b). It can be clearly observed that the wear resistance is improved compared with that of the TC11 substrate. For S-1 (x=25 r/min) and S-2 (x=50 r/min) samples, the wear marks are shallow and clean. Most worn surfaces are relatively smooth. Dispersed WC particles in the coatings are exposed when the surface of the sample is worn, which isolates the matrix from further wear. In addition, the strengthening effect of the WC secondary phase prevents the prepared coating from large deformation, thereby reducing the occurrence of spalling. With the increase in WC content, the deformation and furrows of worn interface are significantly reduced, the interface becomes flatter, and the detrita are also greatly reduced, indicating the improvement of wear resistance. Traces of delamination and peeling of black brittle oxide layer can be observed, which is indicative of typical oxidative wear characteristic according to the EDS analysis shown in Table 3. Oxidative wear, generally slower than adhesive wear, can protect the friction pair. The solid solution strengthening effect of HEA and the strengthening effect of WC particles significantly enhance the hardness and wear resistance of the TC11 surface.

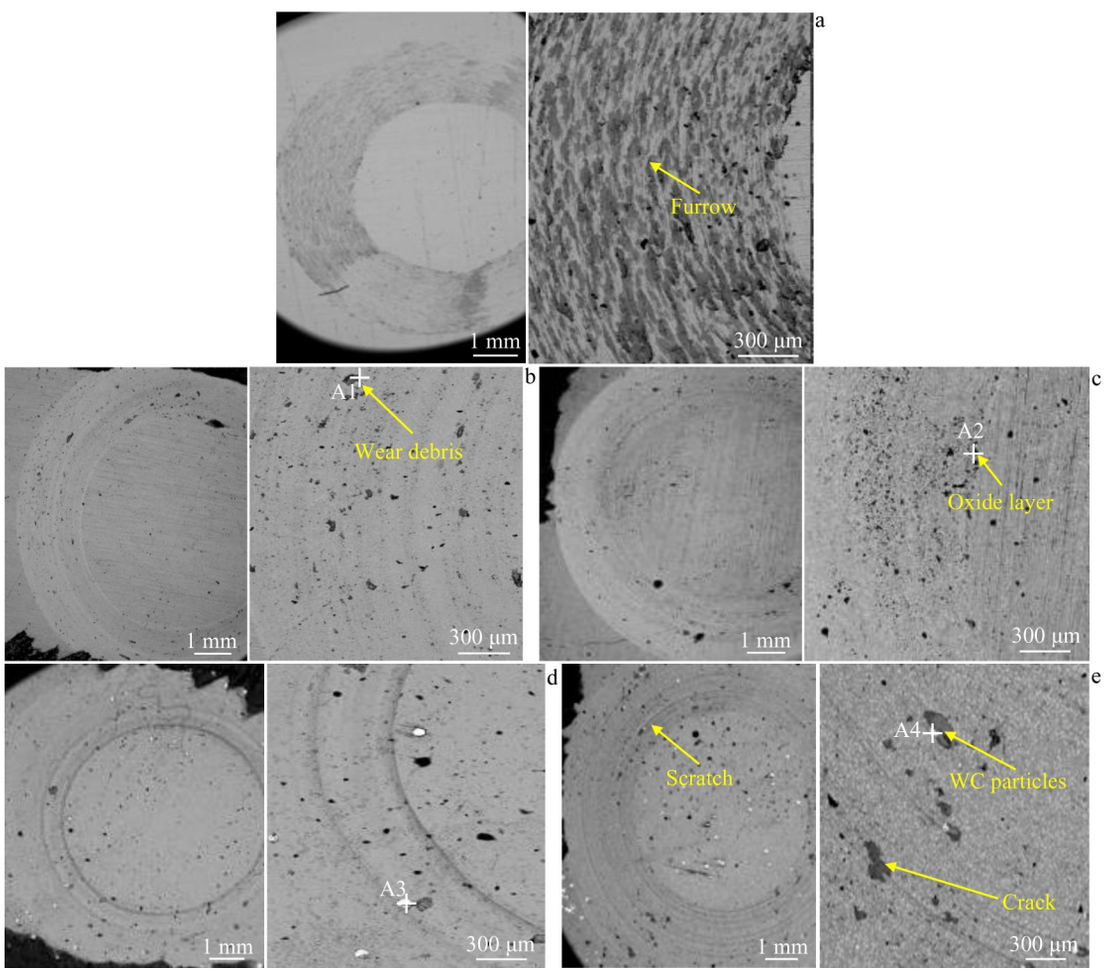

Fig.9 Worn morphologies of $AlCu_2Ti(NiCr)_2$-$(WC)_x$ HEA composite coatings: (a) TC11, (b) S-0, (c) S-1, (d) S-2, and (e) S-3

Table 3 EDS analysis of region A1–A4 marked in Fig.9

Sample	Region	Element/at%							
		Al	Cu	Cr	Ni	C	Ti	W	O
S-0	A1	3.1	19.1	2.7	5.2	-	46.4	-	23.5
S-1	A2	2.9	15.2	2.6	4.3	6.5	43.1	2.1	23.3
S-2	A3	1.1	3.6	0.9	1.9	47.3	23.1	21.0	1.1
S-3	A4	0.6	1.0	0.5	0.9	50.3	1.3	42.7	2.7

For S-3 (x=75 r/min) sample, EDS analysis reveals that the WC particles on the worn surface are not intact and exhibit delamination, indicating fall-off of WC particles during the friction and adhesive wear on the HEA matrix[40]. The unmelted WC spherical particles in the coating contribute to the wear test as a grinding material, reducing wear resistance.

4 Conclusions

1) $AlCu_2Ti(NiCr)_2$-$(WC)_x$ HEA composite coatings can be fabricated through the paraxial input of $AlCu_2Ti(NiCr)_2$ CWW and the coaxial incorporation of WC powder using a robotic plasma cladding system.

2) The produced coatings comprise a mixture of bcc and fcc solid solutions. The solid solution strengthening effect of the HEA, combined with the WC/TiC-based solid solution formed by the added WC during the cladding process, significantly reduces friction.

3) The hardness of the produced coatings is 2.0–2.6 times greater than that of the TC11 substrate. The best wear rate of the composite coating is 32% lower than that of the TC11 titanium alloy.

References

1 Peters M, Kumpfert J, Ward C H *et al. Advanced Engineering Materials*[J], 2003, 5(6): 419

2 Huo X R, Nie S N, Zhang Y W *et al. Chemical Engineering Journal*[J], 2024, 487: 150622

3 Chen D, Cui X F, Guan Y J *et al. Tribology International*[J], 2024, 194: 109534

4 Huang G W, Li L X, Cheng J *et al. Tribology International*[J], 2024, 194: 109480

5 Zheng K K, Zhao X Z, Pan L *et al. Wear*[J], 2024, 550–551: 205415

6 An F P, Zhang L J, Wu J *et al. Materials Characterization*[J], 2024, 212: 113926

7 Wang C J, Yang W, Shao W T *et al. Journal of Materials Research and Technology*[J], 2024, 30: 7663

8 Teng J Z, Jiang P F, Cong Q *et al. Journal of Materials Research and Technology*[J], 2024, 29: 2175

9 Yeh J W, Chen S K, Lin S J *et al. Advanced Engineering Materials*[J], 2004, 6(5): 299

10 Chen Y T, Yang Z D, Xu K *et al. Journal of Materials Research and Technology*[J], 2023, 26: 4191

11 Cheng X M, Yang K, Liu S Z *et al. Transactions of Nonferrous Metals Society of China*[J], 2023, 33(10): 3027

12 Yang Z D, Fang C F, Wu M F *et al. Journal of Materials Processing Technology*[J], 2018, 255: 443

13 Wu Z X, He M J, Feng C S *et al*. *Journal of Thermal Spray Technology*[J], 2022, 31(4): 1244

14 Liao W B, Wu Z X, Lu W *et al*. *Intermetallics*[J], 2021, 132: 107138

15 Liao W B, Xu C H, Wang T L *et al. Vacuum*[J] 2023, 207: 111586

16 Shen Q K, Xue J X, Yu X Y *et al. Surface and Coatings Technology*[J], 2022, 443: 128638

17 Lu B W, Cui X F, Li Y *et al*. *Surface and Coatings Technology*[J], 2017, 319: 155

18 Jambagi S C. *Journal of Alloys and Compounds*[J], 2017, 728: 126

19 Bai H Q, Kang L, Zhang P C *et al*. *Vacuum*[J], 2023, 215: 112336

20 Jung S G, Han Y, Kim J H *et al. Journal of Alloys and Compounds*[J], 2024, 995: 174816

21 Liang G, Jin G, Cui X *et al*. *Applied Surface Science*[J], 2022, 572: 151407

22 Chen Y, Fang C F, Yang Z D *et al. Journal of Manufacturing Processes*[J], 2018, 32: 506

23 Wang Z Q, Shi Y, Zhang Z X *et al. Materials Letters*[J], 2022, 324: 132706

24 Rooprai R S, Bansal A, Singh J. *Tribology International*[J], 2023, 189: 108937

25 Ziejewska C, Marczyk J, Szewczyk-Nykiel A *et al. Advanced Powder Technology*[J], 2019, 30(4): 835

26 Peng Y B, Zhang W, Li T C *et al. International Journal of Refractory Metals and Hard Materials*[J], 2019, 84: 105044

27 Gu D, Ma J, Chen H *et al. Composite Structures*[J], 2018, 192: 387

28 Wang G, Liu X B, Zhu G X *et al. Surface and Coatings Technology*[J], 2022, 432: 128064

29 Yan G H, Zheng M Y, Ye Z H *et al. Journal of Alloys and Compounds*[J], 2021, 886: 161252

30 Sünbül S E. *Journal of Alloys and Compounds*[J], 2024, 996: 174881

31 Kotan H, Polat G, Yildiz A B. *Advanced Powder Technology*[J], 2021, 32(8): 3117

32 Kotan H, Kris D. *Materials Characterization*[J], 2018, 138: 186

33 Liao W B, Wu Z X, Lu W J *et al. Intermetallics*[J], 2021, 132: 107138

34 Wang X R, Wang Z Q, He P *et al. Surface and Coatings Technology*[J], 2015, 283: 156

35 Ma H, Shek C H. *Journal of Alloys and Compounds*[J], 2020, 827: 154159

36 Ye Y Z, Guo Z J, Zhou Z J *et al. Corrosion Science*[J], 2024, 232: 112049

37 Liu F C, Gao J, Liu F G *et al. Tribology International*[J], 2023, 188: 108835

38 Li L Q, Jiang H Q, Liu Y C *et al. Journal of Materials Research and Technology*[J], 2024, 29: 1172

39 Zhang M X, Qin Y, Yang G. *Tribology International*[J], 2024, 192: 109331

40 Peng Y, Zhang W, Li T *et al. Surface and Coatings Technology*[J], 2020, 385: 125326

TC11表面缆式焊丝-粉末等离子熔覆技术制备$AlCu_2(NiCr)_2Ti$-$(WC)_x$高熵合金复合涂层的显微组织和磨损性能

蘧星辰[1]，王小荣[1]，刘晓琴[1]，刘潇潇[1]，孟　倩[2]，何　鹏[3]

(1. 兰州交通大学 机电工程学院，兰州 甘肃 730010)

(2. 兰州交通大学 材料科学与工程学院，兰州 甘肃 730010)

(3. 哈尔滨工业大学 先进焊接与连接国家重点实验室，哈尔滨 黑龙江 150001)

摘　要：采用$AlCu_2(NiCr)_2Ti$缆式焊丝（CWW）和碳化钨（WC）粉末混合模式，通过等离子熔覆技术制备了高熵合金复合涂层$AlCu_2(NiCr)_2Ti$-$(WC)_x$ (x=0, 25, 50, 75 r/min)。研究了WC送粉速度对所制备涂层的显微组织、硬度和磨损性能的影响。结果表明，涂层由体心立方主相和面心立方次相组成，WC的加入形成了碳化物增强相。与基体相比，涂层的硬度和耐磨性能显著提高。当WC送粉速度为50 r/min时，涂层的耐磨性能最佳，体积磨损率最小，为8.5869×10^{-6} $mm^3\cdot N^{-1}\cdot m^{-1}$，极大地改善了TC11表面的磨损性能。CWW和WC粉末在等离子熔覆中的协同输送为制备耐磨性增强的高熵合金复合涂层提供了一种可行的技术支持。

关键词：微观结构；金属及合金；高熵合金涂层；等离子熔覆；CWW-粉末协同输送

作者简介：蘧星辰，男，2000年生，硕士生，兰州交通大学机电工程学院，兰州 甘肃 730010，E-mail：quxingchen729@163.com